Glenoid bone strain after anatomical total shoulder arthroplasty: in vitro measurements with micro-CT and digital volume correlation

Y. Boulanaache[1], F. Becce[2], A. Farron[3], D.P. Pioletti[1] and A. Terrier[1*]

1) Laboratory of Biomechanical Orthopedics, Ecole Polytechnique Fédérale de Lausanne, Lausanne, Switzerland

2) Department of Diagnostic and Interventional Radiology, Lausanne University Hospital and University of Lausanne, Lausanne, Switzerland

3) Service of Orthopedics and Traumatology, Lausanne University Hospital and University of Lausanne, Lausanne, Switzerland

* Corresponding author:
Alexandre Terrier
Laboratory of Biomechanical Orthopedics
Ecole Polytechnique Fédérale de Lausanne
Station 9
1015 Lausanne
Switzerland
Tel: +41 21693 9498
Email: alexandre.terrier@epfl.ch
Article type: Technical note

Word count: 3475 (<=3500)
Keywords: Bone strain; Digital volume correlation; Glenoid; Micro-CT; Total shoulder arthroplasty

Author contribution statement:
Boulanaache: research design, data acquisition, analysis and interpretation, manuscript writing.
Becce: research design, data acquisition, manuscript revision.
Farron: study supervision, in vitro surgery, manuscript revision.
Pioletti: study supervision, manuscript revision.
Terrier: study proposal, design, and supervision, data analysis and interpretation, manuscript writing and revision.

Funding: This study was supported by the Swiss National Science Foundation (SNSF #162766) and “Lausanne Orthopedic Research Foundation” (LORF).

Abstract

Glenoid implant loosening remains a major source of failure and concern after anatomical total shoulder arthroplasty (aTSA). It is assumed to be associated with eccentric loading and excessive bone strain, but direct measurement of bone strain after aTSA is not available yet. Therefore, our objective was to develop an in vitro technique for measuring bone strain around a loaded glenoid implant. A custom loading device (1500 N) was designed to fit within a micro-CT scanner, to use digital volume correlation for measuring displacement and calculating strain. Errors were evaluated with three pairs of unloaded scans. The average displacement random error of three pairs of unloaded scans was 6.1 μm. Corresponding systematic and random errors of strain components were less than 806.0 με and 2039.9 με, respectively. The average strain accuracy (MAER) and precision (SDER) were 694.3 με and 440.3 με, respectively. The loaded minimum principal strain (8738.9 με) was 12.6 times higher than the MAER (694.3 με) on average, and was above the MAER for most of the glenoid bone volume (98.1%). Therefore, this technique proves to be accurate and precise enough to eventually compare glenoid implant designs, fixation techniques, or to validate numerical models of specimens under similar loading.

1. Introduction

Although anatomical total shoulder arthroplasty (aTSA) is an effective surgical treatment for advanced glenohumeral osteoarthritis, aseptic loosening of the glenoid implant remains a major cause of failure and concern [1-4]. While various causes have been identified [3], there are still several open questions, as for example on the optimal glenoid implant design. To answer such questions, in vitro studies are frequently performed.

A few different in vitro measurements have been proposed to analyze the glenoid bone-implant mechanical system. Experimental setups approved by the American Society for Testing and Materials (ASTM) were developed to track the bone-implant relative movement with the help of differential variable reluctance transducers (DVRT) [4, 5]. However, these methods affect the bone structure and are limited to a small set of discreet measurement points. Thus, they do not fully describe the bone-implant behavior. To overcome this limitation, a method combining micro-CT and digital volume correlation (DVC) was proposed to measure micromotion around cementless porcine glenoid implants after aTSA [6]. DVC has already been used to evaluate strain in trabecular bone [7-10], cortical bone [9, 11], whole bones [12-14] after hip arthroplasty and vertrebroplasty, and recently on in situ mice tibiae [15]. DVC was applied to investigate displacements around cadaveric scapulae due to axial loading [16] and very recently in the context of cemented polyethylene glenoid implants [17]. This study reported strain measurements of glenoid bone under concentric, anterior and posterior loading (750 N). Medio-lateral bone strain was measured using DVC before and after implantation. Comparing deformation at a virtual section at 5.7 mm away from glenoid face, the authors found that the implanted glenoid was more deformed than the native glenoid and that anteriorly and posteriorly loaded specimens achieved higher range of strain than the concentric loaded specimen.

Furthermore, in order to correctly interpret DVC measurements, uncertainties must be evaluated. Most previous studies evaluated uncertainties either by a zero-strain analysis (two consecutive unloaded scans) [7-9, 12, 18-20], or by virtually deforming image sets [20, 21]. More recently, different DVC parameters have been compared on the same image sets [19, 20]. These studies showed that precision and accuracy depend on the spatial resolution of images and on DVC settings.

Therefore, the objective of the present study was to develop a technique based on micro-CT and DVC to measure in vitro glenoid bone strain after aTSA. More specifically, a custom loading device was designed to replicate physiological loading after aTSA, optimal parameters of the measurement technique were evaluated, and errors associated with the measurement of displacement and strain were quantified.

2. Methods

2.1. Specimen preparation

A fresh cadaveric scapula (harvested from a 69-year-old female) was obtained from Science Care (Phoenix, AZ, USA), wrapped into saline-moistened gauze (10% phosphate-buffered saline) and vacuum sealed to be stored at -80°C. Preoperative planning was performed using standard-of-care conventional shoulder computed tomography (CT) scans (Discovery CT750 HD, GE Healthcare, Waukesha, WI, USA). Data acquisition settings were: 120 kVp tube potential; 200 mA tube current; 0.7 s gantry revolution time; 64 x 0.625 mm beam collimation; 0.984 pitch. Image reconstruction parameters were: 1.25/0.7 mm section thickness/interval, 488 x 488 μm in-plane spatial resolution; sharp (bone plus) kernel. An anthropomorphic thorax phantom (QRM, Moehrendorf, Germany) with a synthetic humerus (Sawbones, Vashon Island, WA, USA) and saline plastic bags simulating rotator cuff muscles were used to replicate in vivo x-ray attenuation in the experimental setup. The scapula was thawed in saline at room temperature for 24 hours prior to CT scanning and refrozen (-80°C) immediately after.

A senior shoulder surgeon (AF) performed the surgical planning from this CT dataset by using a preoperative planning software (BLUEPRINT™ 3D Planning, Tornier-Wright Medical, Montbonnot-Saint-Martin, France). This planning helped selecting the optimal glenoid implant type, size (AEQUALIS™ PERFORM keeled size S, Tornier-Wright Medical, Montbonnot-Saint-Martin, France) and positioning within the glenoid bone. To avoid beam hardening metal artifacts, the two original metallic radiopaque markers were removed from the keel of the glenoid implant by the manufacturer.

The scapula was thawed in saline at room temperature 24 hours prior to implantation. The implant was cemented (TBCem 3, Class IIb, European Medical Contract Manufacturing, Nijmegen, The Netherlands) within the glenoid bone using patient-specific instruments. The scapula was then vacuum-sealed in saline-moistened gauze and then refrozen (-80°C).

The implanted scapula was thawed in saline at room temperature 24 hours prior to mechanical testing. The implanted scapula needed to fit into an aluminum tube with a diameter of 60 mm, thus requiring cutting. A diamond band saw (312 Pathology Saw, EXAKT Technologies, Oklahoma City, OK, USA) was used to remove the acromion, spine, coracoid process, inferior pillar (23 mm from the center of the glenoid cavity), and medial part (70 mm from the center of the glenoid cavity) of the scapula. The soft tissues were kept in order to preserve the natural moisture of the specimen as much as possible (Figure 1). To center the glenoid within the tube and align the medio-lateral scapular axis with the tube axis, we used a custom 3D printed guide. The specimen was then potted 30 mm deep in polyurethan resin (NEUKADUR MultiCast 20, Altropol Kunstoff, Stockelsdorf, Germany).

2.2. Loading device and micro-CT imaging

A micro-CT loading device was adapted to reproduce a force of 1500 N applied by the humeral component on the glenoid implant [22-25]. To avoid beam hardening metal artifacts, we built a spherical cap of polyether ether ketone (PEEK) to replicate the head of the humeral component. This part was mounted on an aluminum piston, aligned with the tube axis. A 2000 N load cell (LCM202-2KN, Omega Engineering, Stamford, CT, USA) and a NI-USB-9215 acquisition card (National Instruments, Austin, TX, USA) were used to monitor the compressive force. Our loading device induced a complex bone deformation. In the middle axial slice, it appears mainly as a bending strain. This bending was caused by the eccentric (relative to loading axis) fixation of the medial part of the scapula in the cement but especially by the natural curved form of the scapula. The axial force of 1500 N was selected as a maximal worst-case scenario value, derived from instrumented prostheses measurements reporting forces higher than 200 % of body weight during activities of daily living [26], for an average patient weighing 75 kg.

The loading device (Figure 2) containing the specimen was inserted into a micro-CT scanner (Skyscan 1076 in vivo micro-CT, Bruker micro-CT, Kontich, Belgium). We first scanned the unloaded glenoid six times subsequently (mCTi, i = 1, …, 6), for error estimation, also known as zero-strain analysis. The scans were performed consecutively pairwise: mCT1-mCT2, mCT3-mCT4, and mCT5-mCT6. After each scan pair, the specimen was removed from the micro-CT and repositioned. The same scanning position was imperatively kept between two consecutive scans. For strain estimation, the glenoid was scanned first in the unloaded state (mCT7), then in the loaded state at 1500 N (mCT8) after preconditioning (10 cycles at 1500 N) and relaxation delay (10 minutes). Scanning parameters were as follows: 36 μm spatial resolution, 100 kV tube potential, 100 µA tube current, 1 mm aluminum filter, 310 ms exposure time, 0.5° rotation step, 360° scanning, 68 mm scanning width and frame averaging 4. 130 minutes were required to scan the entire glenoid, which required three sub-scans (3x21 mm = 63 mm total longitudinal coverage). Images were reconstructed using a ring artifact reduction of level 2 and beam hardening correction of 80 % (NRecon v1.6.10.4, Bruker micro-CT, Kontich, Belgium).

2.3. Digital volume correlation

DVC was used to estimate 3D displacement maps between each micro-CT scan pair. In each pair, one scan was superimposed to the other by the built-in Euclidean rigid registration of the fixed side (5-mm-thick resin-immersed bone) using Amira 6.7 (FEI SAS, Burlington, MA, USA). All scans were then cropped to include the glenoid bone, but exclude the resin (> 20 mm from the glenoid implant keel) and PEEK sides. A mask was applied on each scan to remove the implant and the soft tissues around the bone and cement. This procedure was performed in Amira. For DVC, Elastix-Transformix open-source registration software [27, 28] was used: Displacement maps were obtained from non-rigid registration with multi-resolution B-spline transform and gradient-descent optimization of normalized correlation coefficient similarity metric. Strain maps were derived from displacement maps using Abaqus finite element solver (v.6.14, Simulia, Dassault Systèmes, Providence, RI, USA).

2.4. Parametric study

To find optimal DVC parameters, a parametric study of 53 different settings was performed. The parameters considered were: grid size, number of resolutions[1], sample size, similarity metric, number of histogram bins and the optimization routine. This optimization was performed on three sets of scan pairs: Set1, Set2, and Set3. Set1 contained two same scans (mCT3-mCT3). Set2 contained an unloaded scan (mCT3) and the same scan virtually deformed (mCT3s) with a stretch of 0.5 % in the three orthogonal directions. Set3 consisted of two repeated unloaded scans (mCT3 and mCT4). From Set1, we rejected all settings producing non-zero displacement. From Set2, we rejected all settings not predicting the controlled stretch. The check was performed visually and quantitatively by computing the median of the resulting strain in the three orthogonal directions (E11, E22, and E33). We kept only settings visually reproducing the applied stretch and with an error below 150 με. This limit was set for convenience in order to limit the number of settings to 3. It is important to mention that although some settings produced the lowest errors, they were not kept if they did not reproduce the applied deformation. From Set3, we chose the settings that produced the lowest random errors for the three displacement components (U1, U2, and U3). The direction of U3 is along the scanning and loading axis, and the other two are orthogonal, approximately corresponding to antero-posterior and infero-superior axes. Details are provided in Supplementary Material A.

[1] "Resolutions" is a term used by the software developers to designate "iterations"

2.5. Error analysis

The errors associated with this measurement technique (optimal DVC parameter set for loaded displacement and strain described above) were evaluated by a zero-strain analysis on the three unloaded micro-CT scan pairs (mCT1-mCT2, mCT3-mCT4, and mCT5-mCT6). Strains were derived from displacement maps on a 2 mm-sized hexahedral mesh of the entire scan. Several errors were evaluated for each of the three scan pairs: We calculated the displacement random errors defined by the standard deviation of the measured displacement. We calculated for each of the six components of strain the systematic and random errors defined respectively by the mean and standard deviation of strain values [19]. Systematic and random errors of the principal strain invariants were calculated. Finally, in order to be consistent with previous studies on DVC, for each scan pair, we evaluated the accuracy and precision defined by the mean absolute error (MAER) and standard deviation of absolute error (SDER) of strain, respectively [7, 19, 29]. An overview of the error analysis described above is presented in Figure 1 of Supplementary Material.

For sake of comparison with other studies, the above mentioned errors were evaluated in a volume of interest (VOI). The VOI (125x226x190 voxels) was located on the anterior part of the glenoid (Figure 3).

2.6 Loaded displacements and strains

Displacements of the loaded scapula were calculated with the optimal DVC parameter set (Appendix A) using unloaded (mCT7) and loaded (mCT8) scans. Strains were derived from displacements on a tetrahedral mesh (2 mm size) of the glenoid bone, which was segmented with Amira. We report the amplitude of displacement and the minimum principal strain stain invariant. All other displacement and strain components are provided in Supplementary Material B.

3. Results

3.1. Parametric analysis

The parametric analysis provided the following optimal parameter set: five-resolution B-spline transform (40-voxel grid size) and gradient-descent optimization (gain factor 100 and 32 histogram bins) of normalized correlation coefficient similarity metric using a sample size of 12’000. Extended data can be found in Supplementary Material A.

3.2. Error analysis

The random error of displacement in all three directions ranged between 2.9 and 11.7 µm. The average random error in loading direction was 6.1 µm and peaked at 9.0 µm. (Figure 3).

The systematic error of the six components of strain ranged between -172.7 µε and 806.0 µε, while random error ranged between 395.3 µε and 2039.9 µε. The systematic error of principal strain invariants ranged between -1367.2 µε and 1348.7 µε, while random error of principal strain invariants ranged between 280.6 µε and 1656.3 µε. On average, systematic and random errors of the third principal strain invariant were -1129.4 µε and 1274.7 µε, respectively.

Over the three zero-strain analysis, the accuracy of the method (MAER) ranged between 484.2 µε and 800.2 µε while the precision (SDER) ranged between 313.2 µε and 579.8 µε. On average, accuracy (MAER) was 694.3 µε, while precision (SDER) was 440.3 µε.

Within the VOI, the random errors of displacement ranged between 1.62 μm and 2.17 μm. The systematic error of the six components of strain ranged between -321.7 με and 637.9 με, while random error ranged between 410.1 με and 964.9 με. The systematic error of the third principal strain invariant was -681.7 με while its random error was 539.4 με. MAER was 626.0 με and SDER was 195.7 με

3.3. Loaded displacement and strain

Maximum displacement amplitude was 825.4 μm (Suppl. Material Table B. 1). Displacement in the axial (loading) direction was up to 797.6 μm (Figure 4, left), while maximum displacement in the transverse direction was 825.4 μm. The axial displacement was greater on the anterior than posterior side, revealing a bending deformation. The bone volume fraction of axial displacement above the average random error of 6.1 μm was 99.6 %.

Minimum principal strain was more negative (compressive) on the anterior than posterior side (Figure 4, right). Average and peak compressive strain (absolute minimum principal strain) were 8738.9. με and 46’000.0 με, respectively. The bone volume fraction of minimum principal strain above accuracy (MAER) was 98.1 % (Figure 5). The minimum principal strain percentile values 5%, 25%, 50%, 75%, 95% were respectively: -22400, -11160, -6540, -3770, -1210 με Extended data can be found in Supplementary Material B.

Discussion

Although total shoulder arthroplasty is an effective procedure to relieve pain and restore range of motion, its failure rate is higher than hip arthroplasty [30, 31]. Component loosening was identified as a possible cause of failure. Loosening may be due to excessive bone deformation. The aim of this study was to develop a method to measure strain within the glenoid bone after aTSA, while a load was applied to the glenoid implant by its humeral counterpart. Micro-CT images and DVC were combined to evaluate glenoid bone strain.

The peak random error of displacement in the loading direction corresponded to 1.1 % of the maximum loaded displacement (797.6 μm). The random error was evenly distributed over the glenoid bone with the exception of localized peaks found at the edges of the bone. At around 3 mm away from the edges, on the VOI, this error decreased to 2.2 μm. The random errors of displacement were in the same range as other DVC studies using similar scanning spatial resolutions: from 0.5 to 63.1 μm random errors [19].

The systematic and random errors of strain were consistent with other similar cemented bone measurements at 16-voxel size, but higher for 48-voxel size [19]. A variability in error values was observed between the three zero-strain tests due to the unavoidable repositioning, as reported by a recent study which found higher errors after repositioning (mean strain differences up to -4427 με). It would have been interesting to report zero-strain errors using two consecutive scans without repositioning but it was not possible due to the size of the

specimen which required three subscans. The specimen holder movement between repeated scans was thus unavoidable.
The reported MAER (626.0 με) and SDER (195.7 με) values on the VOI were within the range of a previous study on cemented specimens (VOI-3 of [19] using DaVis-DC method) but they were higher than a recent in situ study on loaded mouse tibiae that reported MAER and SDER around 158 for an equivalent subvolume[15]. Considering the whole bone, MAER (694.3 με) and SDER (440.3 με) were also in the range of the previous study (VOI-3 and VOI-5 of [19] using DaVis-DC method). The MAER represented 7.2% of the average compressive strains in bone. According to [7], the MAER is below the recommended 10%, thus ensuring the usability of our method for future numerical model validation when expected average minimum principal strain is above 0.6 %. A further error calculation involving repeated virtually deformed scans was performed following a recently published study [32] (Supplementary material, D).

Previous studies on vertebrae, femur and tibia found compressive yield strain to range between 7'000 – 10'000 με [33, 34]. If we assume the glenoid bone to yield around 10'000 με, 72.3 % of our glenoid sample was in the elastic range under 1500 N of compressive axial loading. Although the peak compressive strain value of 46'000 exceeds bone failure strain, it concerned only 0.1% of the bone, was located at the most inferior part of the specimen, at the border to the gauze. This value was thus considered an outlier. Furthermore, the minimum principal strain at percentile 5%, 25%, 50%, 75%, 95% were respectively -22400, -11160, -6540, -3770, -1210 με. Yield strain was reached in some locations, it would be worth performing a third scan in the future, after removal of the load, to evaluate permanent damage.

The non-rigid registration was obtained using the Elastix package, which provides a wide range of parameters to achieve optimal accuracy (presented in Supplementary Material A). All previous studies on bone used B-spline transform for their non-rigid registration with Elastix [35-37]. Elastix indeed recommends a cubic B-spline order. The B-spline function uses a grid on the target image, which the user should refine for each iteration. Conducting a parametric study to determine the optimal registration parameters is critical [38]. In our study, the optimal parameters were obtained by using virtually stretched images and comparing the outcome both qualitatively and quantitatively. Although a stretch instead of compression was applied, it did not change the quality of the transformed image. It was important to stretch the images in the expected deformation directions and by the expected deformation amount in order to optimize the parameters' sensitivity to the applied loading. Registration was obtained within 20 minutes (32 CPUs, 128 GB RAM).

The main strength of this study was to provide original measurements of 3D strain maps within the whole glenoid bone after aTSA. These measurements were obtained using a custom-made loading device, specifically designed for this study. Furthermore, we faithfully replicated the standard clinical surgical setting with the help of preoperative CT scans, preoperative surgical planning software, and patient-specific instruments. We also analyzed the error, by using three consecutive micro-CT scan pairs, instead of the commonly reported analysis performed on single scan pairs only. Another strength of this study was the evaluation of the errors on three different types of scans and especially on a virtually stretched scan, while all previous studies which investigated DVC errors used only one repeated unloaded scan. Besides, our study showed that some DVC parameters can output very small errors for repeated unloaded scans, but may also underestimate the deformation when applied to virtually stretched image. Therefore, we eventually chose DVC parameters providing optimal confidence of the measured deformation after loading, although these parameters did not output the lowest zero-strain error.

In this feasibility study, we applied the technique only to a single sample. In a next step, we will evaluate the variability of the glenoid strain after aTSA with a series of scapulae. A natural variability is indeed expected since the glenoid implant is usually not aligned with the medio-lateral loading axis. For this case, the planned version was 7 degrees (retroversion) and the inclination was zero degrees. In a series of scapulae, the range of glenoid version and inclination should be less than 10 degrees. The measured strain was limited to bone by masking micro-CT images. This masking excluded soft tissue artefacts surrounding the scapula and reduced the measurement errors [19, 39]. The scapula was cut to fit inside the micro-CT, thus affecting its stiffness , if compared to the in vivo state.

In conclusion, this technique provides the 3D maps of displacement and strain within the glenoid bone after aTSA. It is based on a custom-made loading device for micro-CT imaging and DVC analysis, and its accuracy and precision levels are sufficient to eventually compare different surgical techniques (reaming, cementing, implant types) or validate numerical models of similar specimens under high loading magnitude.

Conflict of interest: None of the authors has any conflict of interest.

Acknowledgments: This study was financially supported by the Swiss National Science Foundation (SNSF #162766) and Lausanne Orthopedic Research Foundation (LORF). The authors thank Florian Laboulfie and Vincent Coulange from Tornier-Wright Medical for providing material and technical support.

References

[1] Chevalier Y, Santos I, Muller PE, Pietschmann MF. Bone density and anisotropy affect periprosthetic cement and bone stresses after anatomical glenoid replacement: A micro finite element analysis. Journal of biomechanics. 2016;49:1724-33.

[2] Wee H, Armstrong AD, Flint WW, Kunselman AR, Lewis GS. Peri-implant stress correlates with bone and cement morphology: Micro-FE modeling of implanted cadaveric glenoids. Journal of orthopaedic research : official publication of the Orthopaedic Research Society. 2015;33:1671-9.

[3] Lewis GS, Brenza JB, Paul EM, Armstrong AD. Construct damage and loosening around glenoid implants: A longitudinal micro-CT study of five cadaver specimens. Journal of orthopaedic research : official publication of the Orthopaedic Research Society. 2016;34:1053-60.

[4] Sabesan VJ, Ackerman J, Sharma V, Baker KC, Kurdziel MD, Wiater JM. Glenohumeral mismatch affects micromotion of cemented glenoid components in total shoulder arthroplasty. Journal of shoulder and elbow surgery / American Shoulder and Elbow Surgeons [et al]. 2015;24:814-22.

[5] Nuttall D, Birch A, Haines JE, Watts AC, Trail IA. Early migration of a partially cemented fluted glenoid component inserted using a cannulated preparation system. Bone & Joint Journal. 2017;99-B:674-9.

[6] Sukjamsri C, Geraldes DM, Gregory T, Ahmed F, Hollis D, Schenk S, et al. Digital volume correlation and micro-CT: An in-vitro technique for measuring full-field interface micromotion around polyethylene implants. Journal of biomechanics. 2015;48:3447-54.

[7] Liu L, Morgan EF. Accuracy and precision of digital volume correlation in quantifying displacements and strains in trabecular bone. Journal of biomechanics. 2007;40:3516-20.

[8] Gillard F, Boardman R, Mavrogordato M, Hollis D, Sinclair I, Pierron F, et al. The application of digital volume correlation (DVC) to study the microstructural behaviour of trabecular bone during compression. Journal of the mechanical behavior of biomedical materials. 2014;29:480-99.

[9] Dall'Ara E, Barber D, Viceconti M. About the inevitable compromise between spatial resolution and accuracy of strain measurement for bone tissue: a 3D zero-strain study. Journal of biomechanics. 2014;47:2956-63.

[10] Roberts BC, Perilli E, Reynolds KJ. Application of the digital volume correlation technique for the measurement of displacement and strain fields in bone: a literature review. Journal of biomechanics. 2014;47:923-34.

[11] Christen D, Levchuk A, Schori S, Schneider P, Boyd SK, Muller R. Deformable image registration and 3D strain mapping for the quantitative assessment of cortical bone microdamage. Journal of the mechanical behavior of biomedical materials. 2012;8:184-93.

[12] Hussein AI, Barbone PE, Morgan EF. Digital Volume Correlation for Study of the Mechanics of Whole Bones. Procedia IUTAM. 2012;4:116-25.

[13] Danesi V, Tozzi G, Cristofolini L. Application of digital volume correlation to study the efficacy of prophylactic vertebral augmentation. Clinical biomechanics. 2016;39:14-24.

[14] Tozzi G, Danesi V, Palanca M, Cristofolini L. Elastic Full-Field Strain Analysis and Microdamage Progression in the Vertebral Body from Digital Volume Correlation. Strain. 2016.

[15] Giorgi M, Dall'Ara E. Variability in strain distribution in the mice tibia loading model: A preliminary study using digital volume correlation. Medical engineering & physics. 2018;62:7-16.

[16] Kusins J, Knowles N, Ryan M, Dall'Ara E, Ferreira L. Performance of QCT-Derived scapula finite element models in predicting local displacements using digital volume correlation. Journal of the mechanical behavior of biomedical materials. 2019;97:339-45.

[17] Zhou Y, Gong C, Lewis GS, Armstrong AD, Du J. 3D full-field biomechanical testing of a glenoid before and after implant placement. Extreme Mechanics Letters. 2020;35:100614.

[18] Zhu ML, Zhang QH, Lupton C, Tong J. Spatial resolution and measurement uncertainty of strains in bone and bone-cement interface using digital volume correlation. Journal of the mechanical behavior of biomedical materials. 2016;57:269-79.

[19] Tozzi G, Dall'Ara E, Palanca M, Curto M, Innocente F, Cristofolini L. Strain uncertainties from two digital volume correlation approaches in prophylactically augmented vertebrae: Local analysis on bone and cement-bone microstructures. Journal of the mechanical behavior of biomedical materials. 2017;67:117-26.

[20] Palanca M, Tozzi G, Cristofolini L, Viceconti M, Dall'Ara E. Three-dimensional local measurements of bone strain and displacement: comparison of three digital volume correlation approaches. Journal of biomechanical engineering. 2015;137.

[21] Madi K, Tozzi G, Zhang QH, Tong J, Cossey A, Au A, et al. Computation of full-field displacements in a scaffold implant using digital volume correlation and finite element analysis. Medical engineering & physics. 2013;35:1298-312.

[22] Malfroy Camine V, Rudiger HA, Pioletti DP, Terrier A. Full-field measurement of micromotion around a cementless femoral stem using micro-CT imaging and radiopaque markers. Journal of biomechanics. 2016;49:4002-8.

[23] Gortchacow M, Wettstein M, Pioletti DP, Muller-Gerbl M, Terrier A. Simultaneous and multisite measure of micromotion, subsidence and gap to evaluate femoral stem stability. Journal of biomechanics. 2012;45:1232-8.

[24] Gortchacow M, Wettstein M, Pioletti DP, Terrier A. A new technique to measure micromotion distribution around a cementless femoral stem. Journal of biomechanics. 2011;44:557-60.

[25] Malfroy Camine V, Rudiger HA, Pioletti DP, Terrier A. Effect of a collar on subsidence and local micromotion of cementless femoral stems: in vitro comparative study based on micro-computerised tomography. International orthopaedics. 2018;42:49-57.

[26] Bergmann GGFBARAHABAWP. Orthoload.

[27] Klein S. elastix: A Toolbox for Intensity-Based Medical Image Registration. IEEE TRANSACTIONS ON MEDICAL IMAGING. 2010;VOL. 29, NO. 1.

[28] Shamonin DP, Bron EE, Lelieveldt BP, Smits M, Klein S, Staring M, et al. Fast parallel image registration on CPU and GPU for diagnostic classification of Alzheimer's disease. Frontiers in neuroinformatics. 2013;7:50.

[29] Dall'Ara E, Peña-Fernández M, Palanca M, Giorgi M, Cristofolini L, Tozzi G. Precision of Digital Volume Correlation Approaches for Strain Analysis in Bone Imaged with Micro-Computed Tomography at Different Dimensional Levels. Frontiers in Materials. 2017;4.

[30] Mueller U, Braun S, Schroeder S, Schroeder M, Sonntag R, Jaeger S, et al. Influence of humeral head material on wear performance in anatomic shoulder joint arthroplasty. Journal of shoulder and elbow surgery / American Shoulder and Elbow Surgeons [et al]. 2017;26:1756-64.

[31] Singh JA, Sperling JW, Cofield RH. Revision surgery following total shoulder arthroplasty: analysis of 2588 shoulders over three decades (1976 to 2008). The Journal of bone and joint surgery British volume. 2011;93:1513-7.

[32] Comini F, Palanca M, Cristofolini L, Dall'Ara E. Uncertainties of synchrotron microCT-based digital volume correlation bone strain measurements under simulated deformation. Journal of biomechanics. 2019;86:232-7.

[33] Morgan EF, Keaveny, T.M. Dependence of yield strain of human trabecular bone on anatomic site. Journal of biomechanics. 2001;34:569-77.
[34] Panyasantisuk J, Pahr DH, Zysset PK. Effect of boundary conditions on yield properties of human femoral trabecular bone. Biomechanics and modeling in mechanobiology. 2016;15:1043-53.
[35] Brouwer CL. The effects of computed tomography image characteristics and knot spacing on the spatial accuracy of B-spline deformable image registration in the head and neck geometry. Radiation Oncology. 2014;9:169.
[36] Y. Q. Fast Automatic Step Size Estimation for Gradient Descent Optimization of Image Registration. IEEE TRANSACTIONS ON MEDICAL IMAGING. 2016;35 n2.
[37] Fortunati V, Verhaart RF, van der Lijn F, Niessen WJ, Veenland JF, Paulides MM, et al. Tissue segmentation of head and neck CT images for treatment planning: a multiatlas approach combined with intensity modeling. Medical physics. 2013;40:071905.
[38] Mehrabian H, Richmond L, Lu Y, Martel AL. Deformable Registration for Longitudinal Breast MRI Screening. Journal of digital imaging. 2018;31:718-26.
[39] Pena Fernandez M, Cipiccia S, Dall'Ara E, Bodey AJ, Parwani R, Pani M, et al. Effect of SR-microCT radiation on the mechanical integrity of trabecular bone using in situ mechanical testing and digital volume correlation. Journal of the mechanical behavior of biomedical materials. 2018;88:109-19.

Figure legends

Figure 1. a) Implanted specimen in implantation setup. b) Potted specimen in polyurethan resin. c) image and CAD image of implant

Figure 2. Custom-designed loading device fitting into the micro-CT scanner

Figure 3. Left: Unloaded masked specimen with VOI in orange. Right: Random error of displacement in loading direction (U3).

Figure 4. Top: Loaded unmasked image of specimen (yellow) superposed on unloaded unmasked image of specimen (grey). Bottom: Displacement along loading axis (U3) (left) and minimum principal strain (right) resulting from a 1500 N force applied in the z-direction.

Figure 5. Volumetric distribution of minimum principal strain within the loaded glenoid bone, where the light grey bars represent the accuracy (MAER).

Figure-1

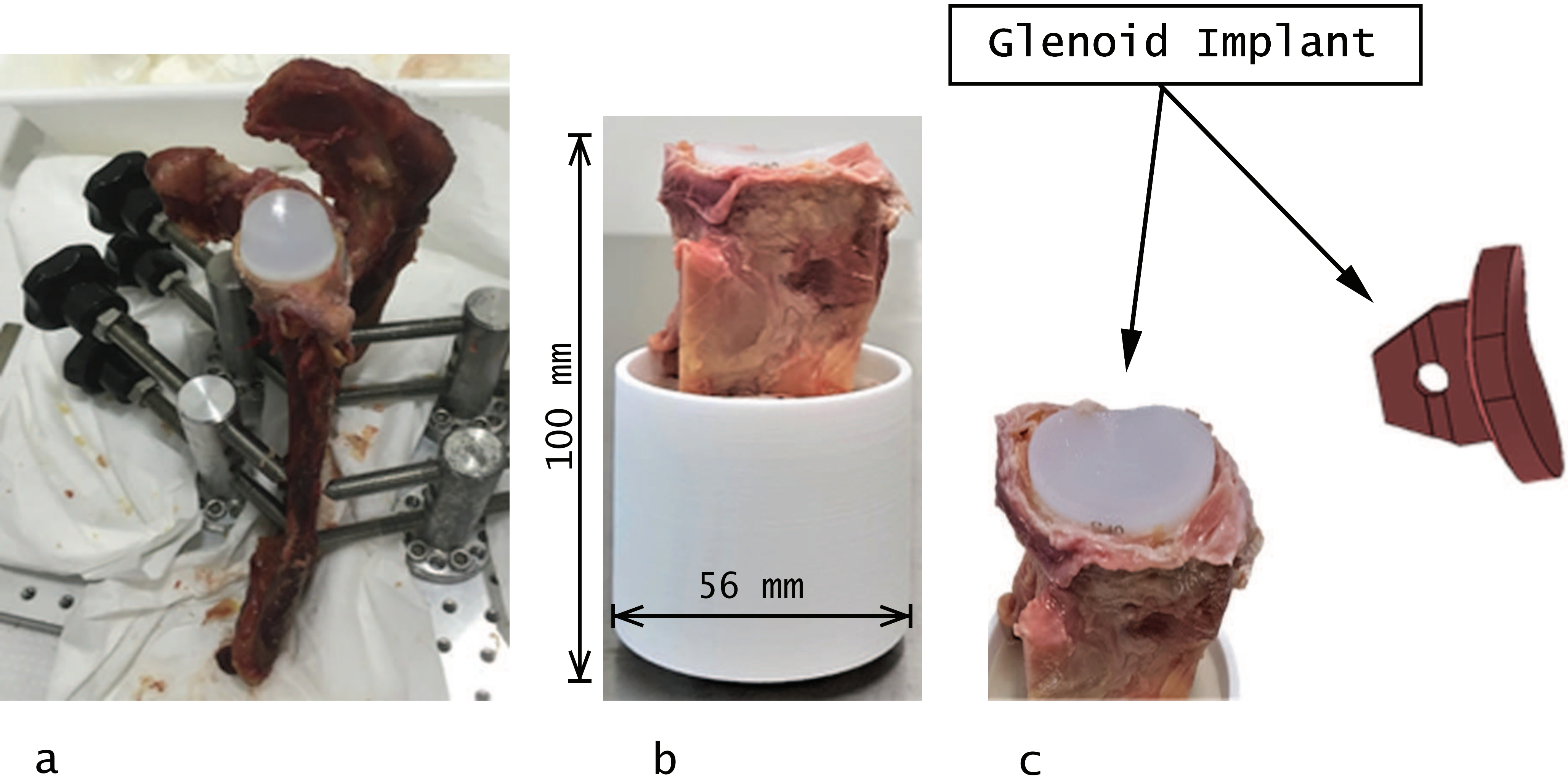

Figure-2

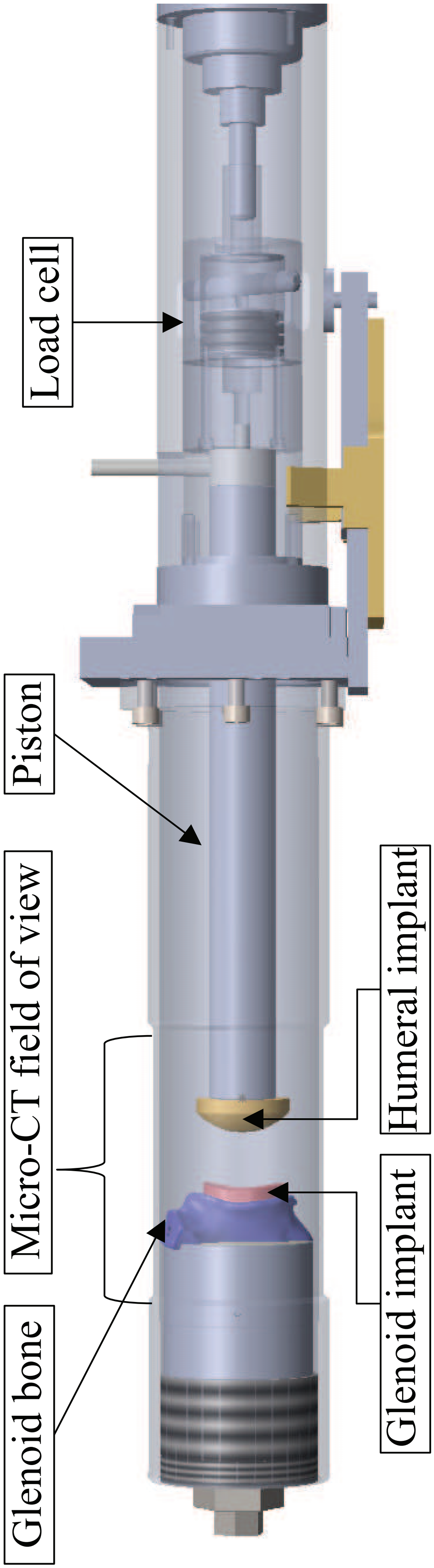

Load cell
Piston
Micro-CT field of view
Humeral implant
Glenoid implant
Glenoid bone

Figure-3

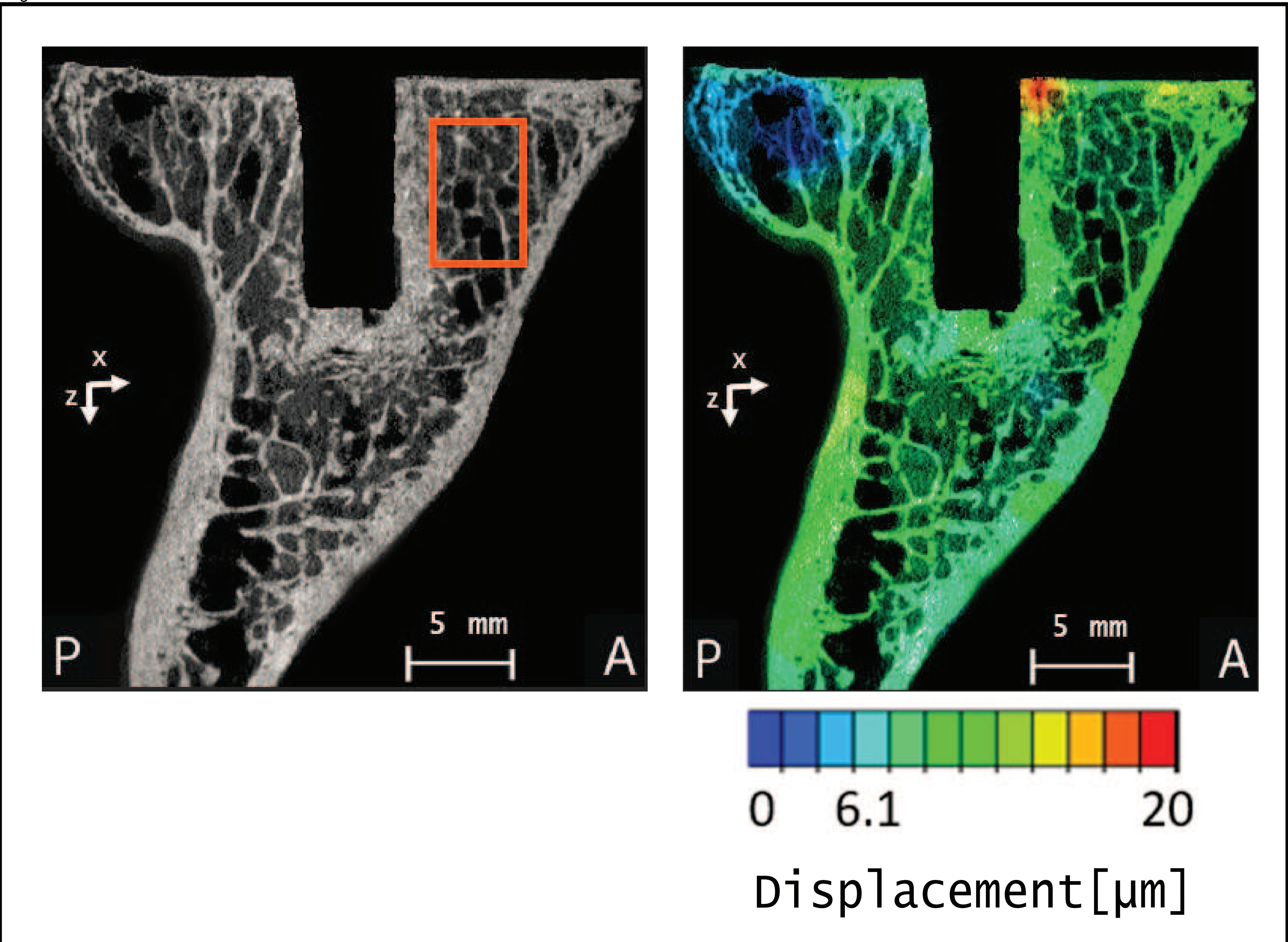

Figure-4

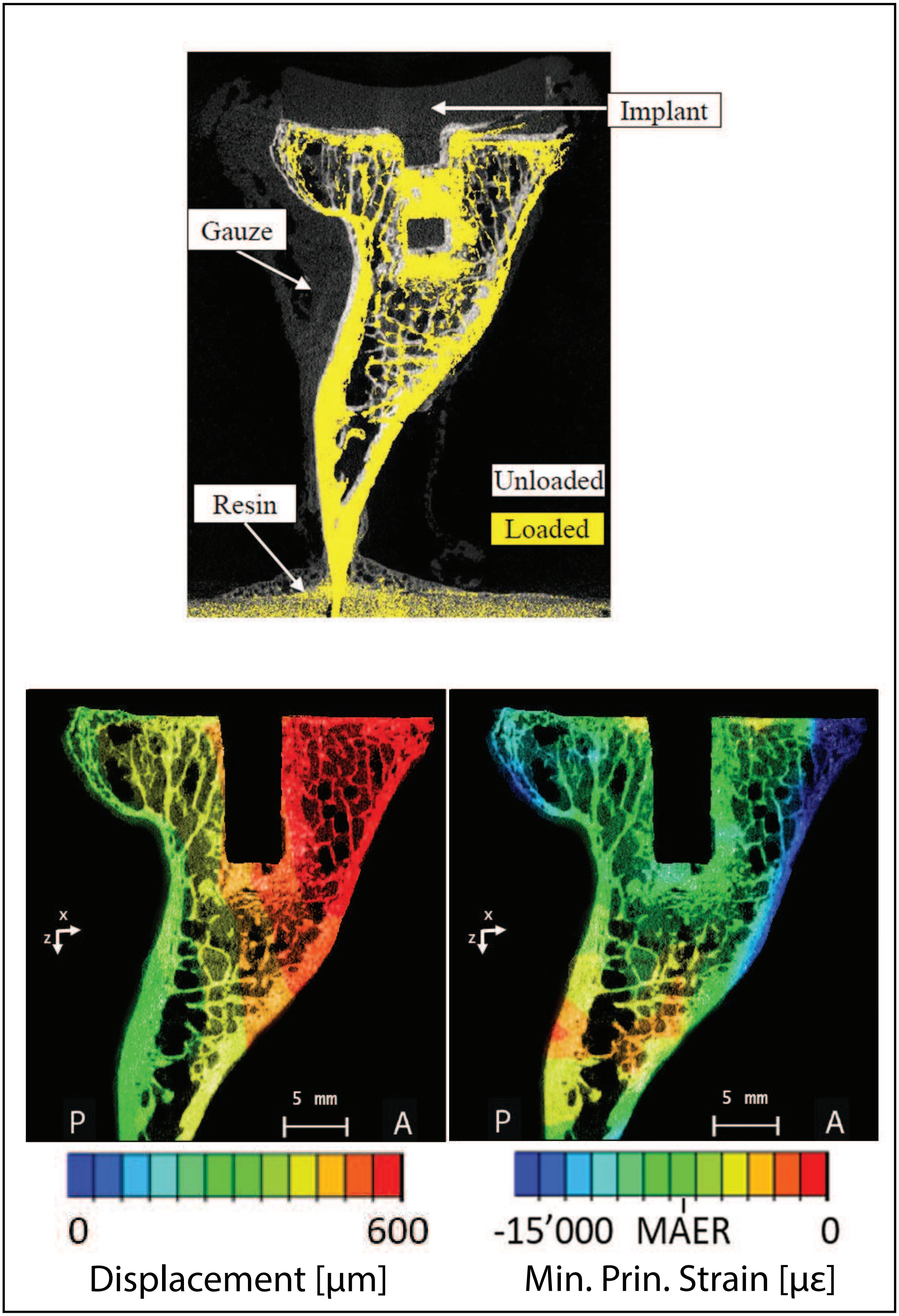

Implant
Gauze
Resin
Unloaded
Loaded
x
z
P
5 mm
A
x
z
P
5 mm
A
0
600
Displacement [μm]
-15’000
MAER
0
Min. Prin. Strain [με]

Figure-5

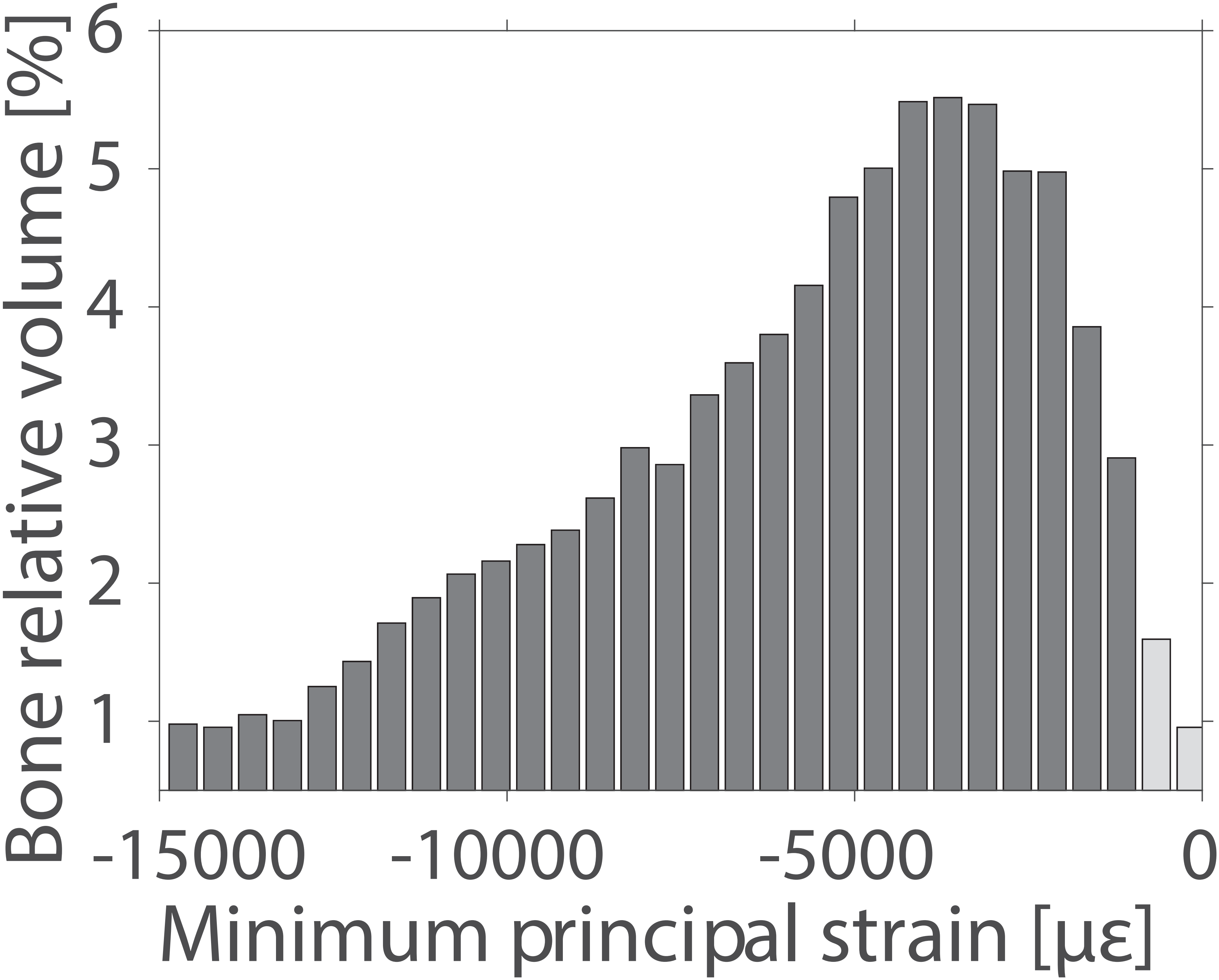
Bone relative volume [%]
6
5
4
3
2
1
-15000
-10000
-5000
0
Minimum principal strain [με]